Effects of Membrane- and Catalyst-layer-thickness Nonuniformities in Polymer-electrolyte Fuel Cells

Adam Z. Weber[1,*,z] and John Newman[1,2,**]

[1]Lawrence Berkeley National Laboratory, Berkeley, California 94720
[2]Department of Chemical Engineering,
University of California, Berkeley, California 94720-1462, USA

In this paper, results from mathematical, pseudo 2-D simulations are shown for four different along-the-channel thickness distributions of both the membrane and cathode catalyst layer. The results and subsequent analysis clearly demonstrate that for the membrane thickness distributions, cell performance is affected a few percent under low relative-humidity conditions and that the position along the gas channel is more important than the local thickness variations. However, for the catalyst-layer thickness distributions, global performance is not impacted, although for saturated conditions there is a large variability in the local temperature and performance depending on the thickness.

* Electrochemical Society Member
** Electrochemical Society Fellow
z E-mail: azweber@lbl.gov

Introduction and Approach

As polymer-electrolyte fuel cells (PEFCs) make the transfer from demonstration to production, manufacturing issues begin to become important. One such issue is that of material-property tolerances, and specifically layer thicknesses. While some thickness variation may be acceptable, the limits are not known. The variation or nonuniformity of layer thicknesses also brings fundamental questions that impact water and thermal management on the cell or global level, and it provides clues as to how durability and degradation may be initiated and proceed on the local level. In this paper, the effect of local variations in the membrane and cathode-catalyst-layer thicknesses in terms of both the local and global performances is investigated.

It is known that manufacturing and production processes inherently result in nonuniform material properties, especially thickness. This variability can be seen in scanning-electron micrographs of the membrane-electrode assembly such as that shown in Figure 1. From multiple micrographs taken from various parts of a PEFC, thickness distributions can be obtained. Figure 2 gives three distributions for both the membrane and cathode catalyst layer, hereby referred to as the catalyst layer, taken from three different PEFCs. A fourth distribution is that of uniform thickness (the solid lines in Figure 2) with values of 13.5 and 30 μm for the catalyst layer and membrane, respectively. In terms of the distributions, for the mathematical analysis, the gas channel was discretized into 32 segments, with every two segments having the same thickness. The distributions clearly show that there is a great deal of variability and randomness in the local thickness values; however, the average values for the different distributions are almost identical as seen in Table I. Table I also gives the standard deviations for each distribution and the cumulative ones, which are essentially normal distributions.

The distributions are for virgin materials; however, it is not expected that they will change in relation to each other upon cell assembly and operation. This is because the gas-diffusion layers are the most compressible, and a simple stress analysis demonstrates that upon membrane swelling and hydration, it is the gas-diffusion layers that will compress.[1-3] It should be noted that the model used accounts for membrane swelling, and the values reported in Table I and Figure 2 are the dry membrane thicknesses.

Mathematical modeling and simulation is ideally suited to examining local effects and properties that are not accessible experimentally, such as how the thickness distributions impact both global and local performance. To do this analysis, we use our previously developed PEFC models.[4,5] The simulations are conducted using a pseudo 2-D approach, where a 1-D cell-sandwich model is run at various segments either along the gas channel in a coflow arrangement, or in a network in a crossflow arrangement as shown in Figure 3. The thickness of either the membrane or catalyst layer is set to a different value in each segment as determined by the distributions shown in Figure 2. As mentioned, for the coflow simulations, a 32-segment discretization is used with identical adjacent points, and for the crossflow simulation, an 8 x 8 discretization is used where each of the 16 2 x 2 areas has the same thickness as taken from Figure 2. The number of segments is chosen such that the simulation results are independent of the number.

The 1-D sandwich is composed of symmetric gas-diffusion layers (GDLs), anode and cathode catalyst layers, and membrane. The parameters and properties of all of the layers except the varying thicknesses are taken from the GDL1 fit in our previous microporous-layer paper.[4] For the heat transfer, the values reported in our previous paper are used,[5] with a heat-transfer coefficient of 1 W/cm^2K (conduction through a typical graphite flow field), and it is assumed

that the outsides of the gas-channel plates are in contact with coolant streams that remain fixed at the inlet temperature (*i.e.*, there is a large coolant flow). Other assumptions are steady-state operation, negligible gravity, local equilibrium (*e.g.*, temperature is the same in all phases at a given location), and liquid-water product.

As noted, the simulations utilize and build on our previous models, and the reader is referred to references 4 and 5 and those contained therein for detailed discussions on the modeling approaches, equations, and parameter expressions as well appropriate historical references. In short, the membrane is treated using our hybrid approach that accounts for transport in both liquid- and vapor-equilibrated membranes for both water and protons. It utilizes concentrated-solution theory and a combined driving force for water movement and accounts for membrane swelling. The catalyst layers are treated using a combined agglomerate-and-porous-electrode approach along with the membrane and GDL models. Thus, proton, gas, and liquid transport is considered throughout their respective phases. The GDLs are treated using our cut-and-rejoin bundle-of-capillaries approach with separate hydrophobic and hydrophilic domains. Liquid flow is modeled using Darcy's law, and gas flow is done with Stefan-Maxwell and Knudsen diffusion along with Darcy's law (*i.e.*, the gas phase is not isobaric). Furthermore, due to the intimate contact between phases, water vapor is assumed to be in equilibrium with the liquid water if present. Nonisothermal phenomena are accounted for by an overall energy balance that contains heat conduction and convection along with heat sources and sinks including water phase change, reversible and irreversible heats of reaction, and Joule heating.

For the boundary conditions, interstitial concentrations and superficial fluxes are continuous between layers. The ionic current density is zero at the GDL / catalyst-layer interfaces, the

electronic current density is zero at the membrane / catalyst-layer interfaces, the electric potential is set equal to zero (arbitrary reference) at the anode GDL / gas-channel interface, and the potential is set to the operating potential at the cathode GDL / gas-channel interface. Simultaneous mass and energy balances are used in the gas channels to obtain the necessary boundary conditions for gas-phase concentrations and temperature.[5] Unless noted below, typical operating conditions are 65°C inlet and coolant temperature, ambient pressure, and 1.2 and 2.0 hydrogen and air stoichiometries, respectively.

The structure of this paper is as follows. First, the effects of the distributions on the local performance are examined for both saturated and low-relative-humidity feeds. This analysis is divided into three subsections, the first dealing with the membrane-thickness distribution, the second with the catalyst-layer-thickness distribution, and the third with upstream effects. Next, the global effects of the variations are examined in terms of overall cell performance for the membrane and catalyst layer under both saturation conditions. Finally, some conclusions are made.

Local Effects

Before proceeding to examine in detail the effects of the local variations, it is of interest to examine how performance is affected by changes in the membrane and catalyst-layer thicknesses in general. To this end, simulations are performed where the thickness was changed uniformly to different values. The resulting impact on performance is shown in Figure 4 in terms of how the cell current density changes at 0.6 V as a function of both the inlet gas humidity and the layer thicknesses, where the range of thickness values encompass the distribution deviations. As expected and discussed in the literature,[6-8] Figure 4 shows that the thinner the membrane, the

higher the current density. Practically, the membrane thickness cannot be too small or gas crossover will become problematic (this occurs at much smaller thicknesses than those shown in Figure 4 and in the distributions in Figure 2). The impact of the membrane thickness is larger for the low-relative-humidity case, where the inlet gases are both fed at 25 % relative humidity, than the saturated case. This is because for the saturated system, the change in membrane thickness has only a minimal impact on performance and system water balance. However, for the low-relative-humidity system, the impact of the membrane thickness has a significant influence due to its effects on the water balance and water management, including humidification of the anode stream, in particular.[9]

Figure 4 also demonstrates that the catalyst-layer thickness impacts performance more significantly than the membrane cases under saturated conditions and less significantly under the low-relative-humidity conditions. Hence, one can say that the system is more oxygen-limited under saturated conditions and water limited under low-relative-humidity conditions. In general, Figure 4 demonstrates that the thicker the catalyst layer, the higher the current density. However, it should be noted that when changing the catalyst-layer thickness all other catalyst-layer parameters are also scaled. Thus, the thicker catalyst layer contains an overall higher loading of platinum. This assumption is used since it seems to agree with the micrographs and also in the distribution studies, where the average loading is similar for the distributions but the local value can vary (see Table I). Because of the above aspect and the range of values explored, the catalyst layer does not demonstrate a maximum in Figure 4 that might be expected due to the additional oxygen and proton mass-transport limitations inherent in a thicker layer.[10,11]

The above treatment and results for the catalyst layer deserves some more discussion. As noted in the literature, both proton or ionic transport and oxygen mass transfer can limit the reaction

rate.[12-14] One could expect that under saturated conditions, oxygen mass transfer is more limiting than proton conduction, and *vice versa* under low-relative-humidity conditions due to dry out of the membrane in the catalyst layer. Thus, although Figure 4 may suggest an infinitely thick catalyst is optimum, if one looks at thicker catalyst layers, a maximum exists even with the higher platinum loadings of the thicker layers. For the saturated conditions this maximum occurs around 100 μm at 0.6 V and drops to 20 μm at 0.3 V due to the more severe oxygen mass-transfer limitations. For the low-relative-humidity case, the optimum is around 40 μm and is mainly caused by the ohmic limitations. The reason why such a thick catalyst layer can be used under these conditions is that the reaction-rate distribution shifts towards the membrane side of the catalyst layer since oxygen is not as limiting. Thus, the protons do not have to travel as far before reacting and much of the catalyst layer is unutilized. Similar analysis has been shown on the anode side of the fuel cell due to the feed of pure hydrogen and the facile hydrogen-oxidation-reaction kinetics.[15,16] Finally, besides the performance aspect, the catalyst layer cannot become too thick due to the economic considerations of platinum.

Membrane-thickness variations.—Figure 5 shows the local, along-the-channel values of the current density and various temperatures for the case of saturated feed gases. From the figure, and in accordance with Figure 4, there are not significant deviations for these cases. In fact, it seems that the position along the gas channel is more important in determining the local values rather than the local membrane thickness, at least in the range in which it is being varied. The current density decreases along the channel mainly due to reactant consumption. The current density has the largest changes near the inlet, which is sensitive to water management in terms of

establishing saturated conditions with steady heat flow, as seen in Figure 5(b) and experimentally in the literature.[17,18]

The temperature distribution is of perhaps more importance from a durability standpoint. As seen in Figure 5(b), and in accordance with the current-density distributions,[17,19] the temperature distributions are also dominated by channel position and not the local thickness. This is especially true for the maximum temperature (which occurs in the cathode catalyst layer) and the anode-gas-channel temperature. The cathode-gas-channel temperature has the largest deviations due to the way in which the energy balance is affected by evaporation and condensation and the water balance as well as the heat conduction through the membrane. For the saturated case, the temperatures increase near the inlet because of the lack of a sufficient heat flux to the coolant due to the low temperature difference, and then the temperatures decrease because of the smaller heat generation due to the lower current density. Figure 5(b) also demonstrates that there are temperature gradients of a couple of degrees within the cell sandwich; the average cell temperature is also a few degrees above that of the coolant stream.

Similar to Figure 5, Figure 6 displays the local current density and temperature set for the case of 25 % relative-humidity feeds. For this case, the performance is mainly dictated by the humidification increase along the channel rather than reactant consumption. However, near the outlet, saturated conditions exist, and the current density decreases in the same manner as in Figure 5(a), which follows trends scene in experimental data.[18,20] The inset graph in Figure 6(b) clearly shows that the current density tracks with the relative humidity of the gas streams. Furthermore, as for the saturated case, it seems that the position along the gas channel is again more important than the local thickness.

For the low-relative-humidity case, the temperature distribution is very different and the effect of the local membrane variations much smaller. In fact, until a liquid-water phase forms, there is no appreciable temperature difference in the cell sandwich from that of the coolant, *i.e.*, the cell is isothermal. This is interesting since the current-density distribution is highly nonuniform, and it underscores the point that water phase changes comprise very large heat sources and sinks. This last point is clearly shown in the way that the temperature changes once liquid water exists near the outlet. However, one must also recognize that, for the drier conditions, there is also less heat generation due to the lower current density and lower reaction overpotential since the liquid water formed evaporates and thus consumes some of the reaction heat. This latter phenomenon is the same as if water vapor is assumed to be the product with the corresponding lower enthalpy potential.

It is clear that the water balance is much more important for the low relative-humidity case. Because of this, one expects larger deviations than for the saturated case. While Figure 6 seems not to demonstrate this point, it is somewhat unfair to compare the values over such a broad current-density range. To examine the deviations more fairly, the logarithm of the current density is plotted in Figure 7(a). Thus, one can see that the deviations near the drier inlet are indeed larger from a percentage standpoint. Furthermore, since the water balance is more critical, it is instructive to examine the dimensionless net water flux through the membrane along the channel. This flux is nondimensionalized by the current density through that segment, and the resulting so-called β value is given in Figure 7(b). It is clear that the impact of the membrane thickness on the local β value is much more significant and dominant than for either the current density or temperature. Furthermore, the $\tilde{\beta}$-value curve shape and mainly negative values are caused by the strong influence of the anode humidity on the water balance.[9] The dip in β where

liquid water appears is due to the changes in temperature at that point. As shown in Figure 6(b), the temperature increases when liquid water forms. This increase in temperature results in a condition where to humidity the anode requires water to move from the cathode (*i.e.*, in a transient sense it is underhumidifed due to the increased temperature) and the resulting β is negative. Overall, for the membrane thickness variations, there are not substantial deviations in the local performance, and the along-the-gas-channel trend is dominant, although, for unsaturated conditions, the influence of the thickness on water management does cause some deviations, especially in the water balance and dry inlet region.

Catalyst-layer-thickness variations.—The previous section demonstrates that the membrane thickness causes some minor deviations in local performance, especially under unsaturated conditions. From Figure 4, one expects the catalyst-layer deviations to be greater than the membrane ones for the saturated case, and lower for the low relative-humidity case. First, the saturated case is examined again in terms of the current density and various temperatures; these plots are given in Figure 8.

For the saturated case, one sees much greater local variations than in any of the previous plots. Instead of being dominated by position along the gas channel, the performance is also very strongly correlated to the local catalyst-layer thickness, especially for distribution 3. Furthermore, the area near the outlet region shows larger deviations due to the more oxygen-limited system that exists there. The temperature profiles also show greater deviations than for the membrane-thickness analysis (compare to Figure 5), although the maximum temperature is now more sensitive than the cathode-gas-channel one. This is due to the fact that the maximum temperature is in the catalyst layer and the cathode-gas-channel temperature is a stronger

function of the water balance, although it does vary locally somewhat for the catalyst-layer thickness distributions. The comparative analyses clearly demonstrate that the catalyst-layer thickness has a greater impact on the local performance than the membrane thickness, above and beyond the fact that the deviations are slightly larger on a percentage basis for the catalyst layer (see Figure 2).

The deviations in both current density and especially the maximum temperature for the saturated cases in Figure 8 could be a concern in terms of lifetime and durability, although the absolute magnitudes of the changes are still relatively minor. However, the heterogeneities that they represent demonstrate unequal heating (*i.e.*, hot spots) as well as different reactant utilization and water management. Such nonuniformities result in concerns of unequal stressing of the various components, with the most important probably being the membrane. While the magnitudes seen in Figure 8 may not be a major concern, these nonuniformities will become larger at higher current densities. They may also cause difficulties and accentuate local failure mechanisms during transient operation and cycling conditions. Finally, it should be remarked that at a certain point the deviations may become large enough in magnitude that the pseudo 2-D assumption breaks down, in which case a full 2-D simulation would be required.

As a final study, Figure 9 shows the current-density deviations for the catalyst-layer thickness distributions with low-relative-humidity feeds. As predicted, there are essentially no deviations, especially for the dry inlet region. This is because this region is not really reaction limited; it is more a function of the water balance, as discussed above. Similar to the results in Figure 6, as the humidity increases and liquid water is formed, the deviations become similar to those witnessed for the saturated case. Thus, for the catalyst-layer thickness, there are large local variations for saturated or near-saturated conditions, and essentially none for unsaturated

conditions. As discussed previously, the thickness variations occur in a range where the increased ionic resistance in the catalyst layer with increased thickness is not controlling since the reaction-rate distribution is shifted towards the membrane and the entire catalyst layer is not being utilized.

Upstream effects.—The previous sections demonstrate that there are some local performance variations due to the variability in the membrane and catalyst-layer thicknesses. One question that can be asked is whether the deviations at a specific point in the gas channel are due just to having the different thickness at that point, or whether they are also due to a propagation of the upstream variations. To answer this question, one can normalize the deviations from Figure 5, Figure 6, Figure 8, and Figure 9 and plot them versus the normalized thicknesses at each point calculated from Figure 2. Figure 10 gives the plot from the simulations for both feed conditions and layer-thickness distributions. A note should be made that, for the membrane thicknesses, the actual wet or swollen membrane thickness is used to calculate the thickness deviations instead of the dry values given in Figure 2. The use of the swollen thickness removes scatter that is due to normally occurring different hydration values; in essence, using the swollen thickness normalizes the data to that of the uniform-distribution case.

For the saturated conditions, the simulation deviations lie more-or-less along a straight line, as seen in Figure 10(a). Furthermore, these lines have slopes that are consistent with those in Figure 4, as expected. The scatter in the simulation points is an indication of the upstream and nonlinear effects in that the local deviations are not consistent with just having a different thickness. It should be noted that while these effects will cause scatter in the plot, there could be more downstream interactions in reality than are accounted for since the pseudo 2-D approach

only links the adjacent segments through mass and energy balances. To ascertain the upstream effects accurately, one should do a full 2-D model. However, it is believed that most of the important ones are captured in the pseudo 2-D approach used here, especially since the flow is coflow. In other words, the most important upstream effects deal with changes in the mass and energy balances (for example, a different humidification profile caused by an altered water balance upstream), which are considered in the pseudo 2-D model.

Since most of the effects are due to mass and energy balances, it is reasonable that for saturated conditions there would not be substantial upstream interactions. However, one would expect many more for the low-relative-humidity cases, and this is exactly what one sees in Figure 10(b). For both the membrane- and catalyst-layer-thickness distributions, there is a lot of scatter. For the membrane, the same general trend is there as in Figure 4, except that the simulation points are much more spread out. This indicates that the changes in the water management upstream are affecting the downstream values although slightly less than having the different local thickness. For the catalyst layer, one cannot find a significant correlation. Some of the points seem to fit into the expected trend and shape, and these are the ones at the more saturated conditions. However, the rest of the points are describing the fact that the current density is not correlated to the catalyst-layer thickness for the dry conditions, as witnessed in Figure 9. Thus, the deviation is essentially zero even though the catalyst-layer thickness changes. Overall, one sees much more upstream effects at low humidities, although they are still not as significant as the local thickness value. Finally, although only the current-density deviations are shown Figure 10, the cathode-gas-channel temperature deviations result in essentially the same figures since the temperature and current density are almost linearly related in this analysis.

Global Effects

The above analysis is focused on how the thickness distributions impact the local performance. Before concluding, remarks should be made on how the global performance is impacted. To do this comparison, the deviation from the uniform case of the average value of the current density from the above figures is calculated for each distribution. Table II summarizes these results as well as those under some other operating conditions and crossflow instead of coflow. From the table it is clear that the deviations for both thicknesses do not have an appreciable impact on the overall performance. This is not unexpected since the average thicknesses are essentially the same as that of the uniform distribution (see Table I). However, it is also somewhat disconcerting considering the deviations seen in the local performances. This is of particular concern in the catalyst-layer, where the larger local deviations (see Figure 8) do not result in any measurable change in the overall current density. Thus, while the overall performance may look good, there still could be local variations which can result in durability and performance issues. In other words, the global performance cannot be used as a signature to detect local problems and nonuniformities, until probably too late, *i.e.*, after significant damage has occurred.

For the membrane cases, Table II shows that the saturated feed conditions do not show a significant impact on the overall performance. For the low-relative-humidity cases, larger deviations are seen as expected from the impact of membrane thickness on the water balance (see Figure 4) as well as the larger amount of upstream effects (see Figure 10). This is interesting because it is essentially the opposite to that of the catalyst layer, since even though the local variations are not large (see Figure 5 and Figure 6) compared to the overall trends, they

are significant enough to change the global current density a couple of percent. When the amount of dry gases is increased by raising the stoichiometry or the temperature, then the current-density deviation also increases due to the larger area of unsaturated gases.[21] Overall, the membrane deviations are still relatively minor, and they more-or-less follow the same trend compared to each other as the average thickness of the distributions (see Table I).

To assess the impact of flow geometry, the above simulations are run in a crossflow instead of coflow arrangement (see Figure 3). As seen in Table II, for the membrane cases, crossflow typically results in smaller global deviations because the flow arrangement allows for better water management, resulting in more efficient saturation of the inlet gases; in fact, the current density for the 25 % relative-humidity crossflow arrangement is typically 30 % larger than for the coflow one. For the catalyst-layer cases, the distributions again demonstrate deviations that are more in accordance with the saturated values; however, they are much larger owing to the nonuniform current-density distribution. Overall, the cell current-density deviations are largest for the low-relative-humidity-feed cases, and one would expect similar variability of around a few percent or so in experimental data that could be directly due to manufacturing nonuniformity in the various layer thicknesses. Finally, as shown in the bottom of Table II, when both distributions are accounted for, the effects are essentially additive. This demonstrates that the membrane and catalyst-layer thickness variations do not interact significantly with each other for the given ranges investigated.

The results discussed above are for a cell potential of 0.6 V. Obviously, one may wonder if the above conclusions and analysis are valid throughout the operating-potential window. To examine this, complete polarization curves are run using the membrane-thickness distributions under both feed humidity conditions, as shown in Figure 11. As expected from Table II, the

saturated-feed cases resulted in only small deviations for the cell performance. Larger deviations are witnessed for the low-relative-humidity feeds, especially in the mass-transport part of the curve where water management becomes much more critical. Furthermore, the nonuniform-distribution cases result in better performance that the uniform case, demonstrating that the impact of thinner membranes is greater than that of thicker membranes. Overall, the deviations are consistent and one expects the conclusions reached above to be generally applicable to any potential. As a side note, polarization curves with the catalyst-layer-thickness distribution demonstrate no noticeable deviation in the curves, which is consistent with the above analysis and Table II.

Conclusions

Simulations with various membrane and cathode-catalyst-layer thickness distributions, determined from experimental, were accomplished. Results indicated that having the nonuniform membrane thickness only marginally affected the local performance; the location of a point along the gas channel was more important than the actual deviation in membrane thickness. The impact of membrane thickness on water management caused larger deviations under unsaturated conditions, as well as more upstream influence on downstream values. Globally, the performance was affected a few percent with drier feeds and lower potentials. For the catalyst-layer-thickness distributions, the global performance was not significantly altered, and there were not significant upstream effects. However, unlike for the membrane-distribution cases, the local performances for cathode-catalyst-layer cases were much more dominated by the local variations. Thus, these deviations are not seen in the overall cell performance and could

result in problems in terms of durability and temperature heterogeneities, especially under more oxygen-limited conditions such as low stoichiometries and saturated conditions.

Acknowledgments

This work was supported by the Assistant Secretary for Energy Efficiency and Renewable Energy, Office of Hydrogen, Fuel Cell, and Infrastructure Technologies, of the U. S. Department of Energy under contract number DE-AC02-05CH11231. Plug Power and Dr. Richard Pollard are acknowledged for providing the experimental distribution data.

References

1. A. Z. Weber and J. Newman, *AIChE J.*, **50**, 3215 (2004).
2. W. K. Lee, C. H. Ho, J. W. Van Zee, and M. Murthy, *J. Power Sources*, **84**, 45 (1999).
3. J. Ge, A. Higier, and H. Liu, *J. Power Sources*, **159**, 922 (2006).
4. A. Z. Weber and J. Newman, *J. Electrochem. Soc.*, **152**, A677 (2005).
5. A. Z. Weber and J. Newman, *J. Electrochem. Soc.*, **153**, in press (2006).
6. B. Andreaus, A. J. McEvoy, and G. G. Scherer, *Electrochim. Acta*, **47**, 2223 (2002).
7. F. N. Büchi and G. G. Scherer, *J. Electrochem. Soc.*, **148**, A183 (2001).
8. D. R. Sena, E. A. Ticianelli, V. A. Paganin, and E. R. Gonzalez, *J. Electronanal. Chem.*, **477**, 164 (1999).
9. G. J. M. Janssen and M. L. J. Overvelde, *J. Power Sources*, **101**, 117 (2001).
10. D. T. Song, Q. P. Wang, Z. S. Liu, T. Navessin, M. Eikerling, and S. Holdcroft, *J. Power Sources*, **126**, 104 (2004).
11. M. Eikerling and A. A. Kornyshev, *J. Electronanal. Chem.*, **453**, 89 (1998).
12. F. Jaouen, G. Lindbergh, and G. Sundholm, *J. Electrochem. Soc.*, **149**, A437 (2002).
13. Q. P. Wang, D. T. Song, T. Navessin, S. Holdcroft, and Z. S. Liu, *Electrochim. Acta*, **50**, 725 (2004).
14. M. L. Perry, J. Newman, and E. J. Cairns, *J. Electrochem. Soc.*, **145**, 5 (1998).
15. M. S. Wilson, J. A. Valerio, and S. Gottesfeld, *Electrochim. Acta*, **40**, 355 (1995).
16. E. A. Ticianelli, J. G. Beery, and S. Srinivasan, *J. Appl. Electrochem.*, **21**, 597 (1991).
17. M. Wilkinson, M. Blanco, E. Gu, J. J. Martin, D. P. Wilkinson, J. J. Zhang, and H. Wang, *Electrochemical and Solid State Letters*, **9**, A507 (2006).
18. Z. Liu, Z. Mao, B. Wu, L. Wang, and V. M. Schmidt, *J. Power Sources*, **141**, 205 (2005).
19. S. Basu, M. W. Renfro, H. Gorgun, and B. M. Cetegen, *J. Power Sources*, **159**, 987 (2006).
20. H. C. Ju, C. Y. Wang, S. Cleghorn, and U. Beuscher, *J. Electrochem. Soc.*, **152**, A1645 (2005).
21. F. N. Buchi, A. B. Geiger, and R. P. Neto, *J. Power Sources*, **145**, 62 (2005).

Captions

Figure 1. Scanning-electron micrograph of a portion of a virgin membrane-electrode assembly showing the various thicknesses for the membrane and catalyst layer.

Figure 2. Experimentally determined distributions of dry membrane (a) and catalyst-layer (b) thickness (and percent deviation) as a function of gas-channel position. Shown are three distributions for each layer and the uniform-distribution value (the zero value).

Figure 3. Schematic of the modeling domain where the 1-D (through-plane) sandwich model is run along the gas channel in coflow or in a 2-D matrix in crossflow. Each 1-D model segment contains a different membrane or cathode-catalyst-layer thickness as given by the distributions in Figure 2.

Figure 4. Impact of catalyst-layer (solid) and membrane (dashed) thickness on the cell current density at 0.6 V. Each thickness is uniform along the gas channel, and the normalization is with respect to the average thicknesses of 30 and 13.5 μm for the membrane and catalyst layer, respectively. The two sets of lines indicate saturated and 25 % relative-humidity feeds.

Figure 5. Along-the-channel values for the (a) current density and (b) maximum and anode- and cathode-gas-channel temperatures as a function of membrane-thickness distribution at 0.6 V with saturated feeds. The distributions correspond to those shown in Figure 2, the solid line indicates a uniform thickness at a value of 30 μm, and the coolant temperature is 65°C.

Figure 6. Along-the-channel values for the (a) current density and (b) maximum and anode- and cathode-gas-channel temperatures as a function of membrane thickness distribution at 0.6 V with 25 % relative-humidity feeds. The distributions correspond

to those shown in Figure 2, the solid line indicates a uniform thickness at a value of 30 μm, and the coolant temperature is 65°C. The inset graph in (b) shows the along-the-channel water partial pressure in the anode and cathode gas channels.

Figure 7. Along-the-channel values for the (a) current density and (b) dimensionless net water flux in the membrane, β, as a function of membrane thickness distribution at 0.6 V with 25 % relative-humidity feeds. (a) is the same as Figure 6(a) except on a logarithmic scale to emphasize the relative errors. The distributions correspond to those shown in Figure 2, and the solid line indicates a uniform thickness at a value of 30 μm.

Figure 8. Along-the-channel values for the (a) current density and (b) maximum and anode- and cathode-gas-channel temperatures as a function of catalyst-layer thickness distribution at 0.6 V with saturated feeds. The distributions correspond to those shown in Figure 2, the solid line indicates a uniform thickness at a value of 13.5 μm, and the coolant temperature is 65°C.

Figure 9. Along-the-channel values for the current density as a function of catalyst-layer thickness distribution at 0.6 V with 25 % relative-humidity feeds. The distributions correspond to those shown in Figure 2, and the solid line indicates a uniform thickness at a value of 13.5 μm.

Figure 10. Normalized current density as a function of normalized layer thickness from simulation for both the membrane (hollow symbols) and catalyst-layer (filled symbols) thickness distributions at 0.6 V with (a) saturated and (b) 25 % relative-

humidity feeds. The normalization is done with respect to the along-the-channel-value deviations from the uniform-thickness-distribution cases.

Figure 11. Polarization curves for the four membrane-thickness distributions for both the (a) 25 % relative-humidity and (b) saturated feed cases.

Table I. Statistical data for the three thickness distributions and the cumulative total of them given in Figure 2 for both the membrane and catalyst-layer.

Table II. Average cell current-density deviations (with respect to the uniform distribution case) under various conditions at 0.6 V for the three thickness distributions of the membrane and catalyst layer. Also included are the deviations when both the membrane and catalyst-layer distributions are considered.

Table I. Statistical data for the three thickness distributions and the cumulative total of them given in Figure 2 for both the membrane and catalyst-layer.

Distribution	**Average (μm)**	**Standard deviation (μm)**
Membrane		
1	29.4	3.6
2	30.8	2.7
3	29.2	3.0
Cumulative	29.8	3.2
Catalyst layer		
1	13.6	2.5
2	13.5	2.1
3	13.4	2.4
Cumulative	13.5	2.3

Table II. Average cell current-density deviations (with respect to the uniform distribution case) under various conditions at 0.6 V for the three thickness distributions of the membrane and catalyst layer. Also included are the deviations when both the membrane and catalyst-layer distributions are considered.

Condition	**Current-density deviation (%)**		
	Dist. 1	**Dist. 2**	**Dist. 3**
Membrane			
Saturated	0.265	0.014	0.258
Low RH	2.55	1.00	2.25
Low RH at 2x stoich.	3.82	0.881	3.84
Low RH at 80°C*	3.26	0.753	3.30
Low RH with crossflow	1.74	0.260	1.59
Catalyst layer			
Saturated	0.110	0.079	–0.231
Low RH	–0.013	–0.072	0.234
Low RH with crossflow	0.085	0.390	0.493
Membrane + Catalyst Layer			
Saturated	0.414	0.107	0.019
Low RH	2.71	0.931	3.05

* Both inlet and coolant temperature

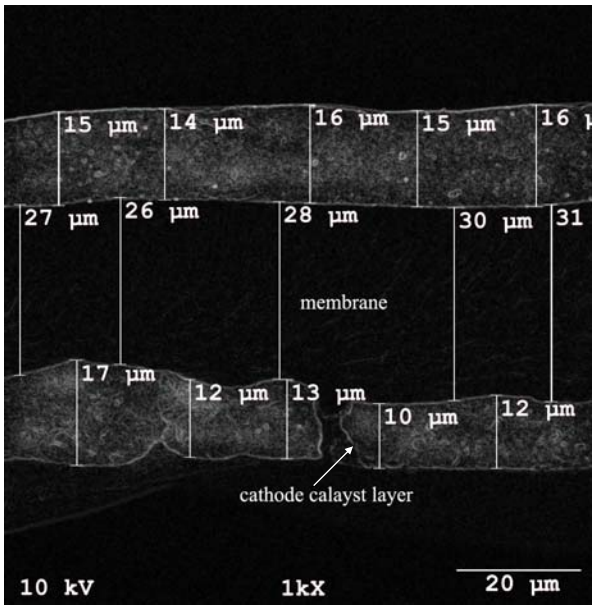

Figure 1. Scanning-electron micrograph of a portion of a virgin membrane-electrode assembly showing the various thicknesses for the membrane and catalyst layer.

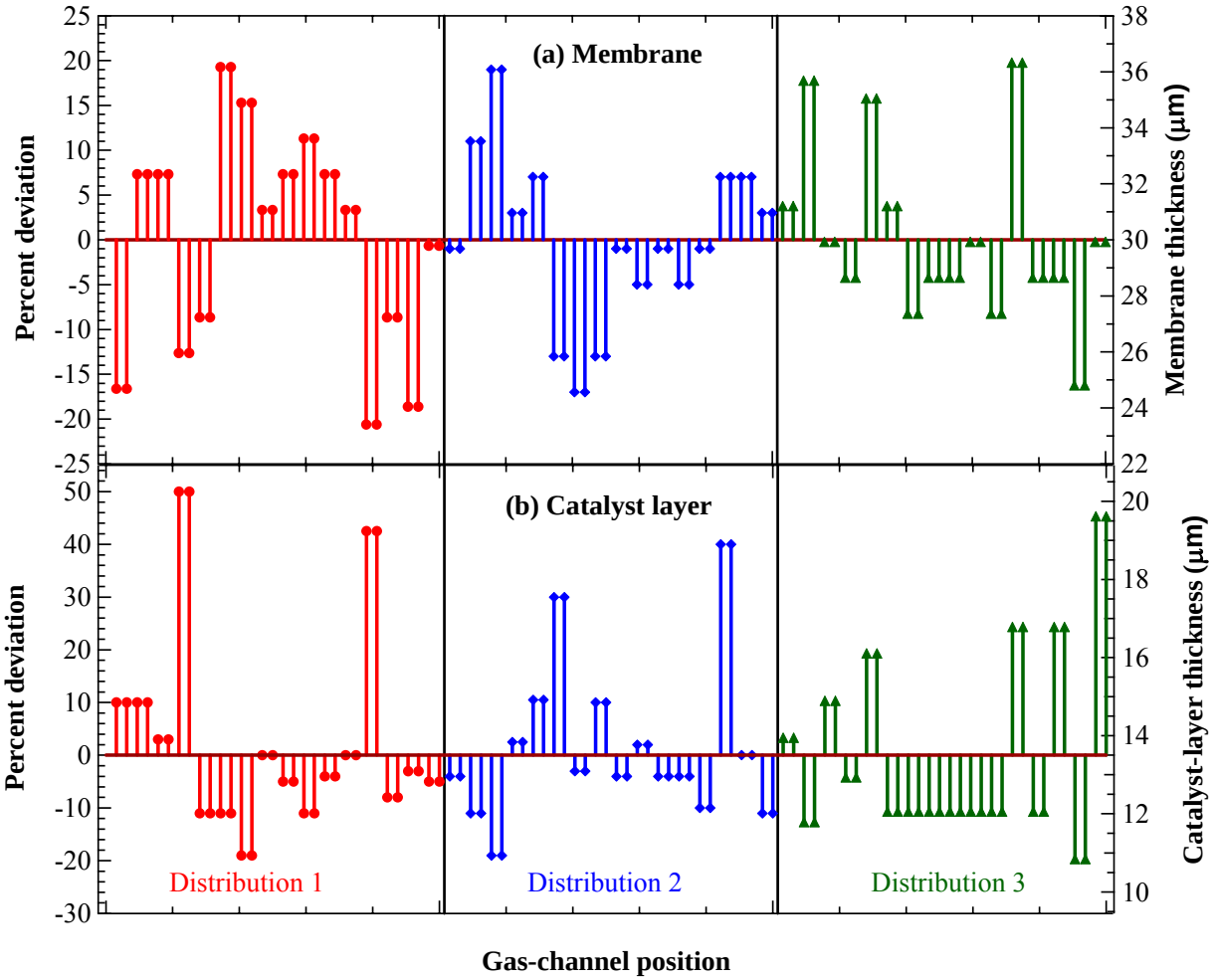

Figure 2. Experimentally determined distributions of dry membrane (a) and catalyst-layer (b) thickness (and percent deviation) as a function of gas-channel position. Shown are three distributions for each layer and the uniform-distribution **value (the zero value).**

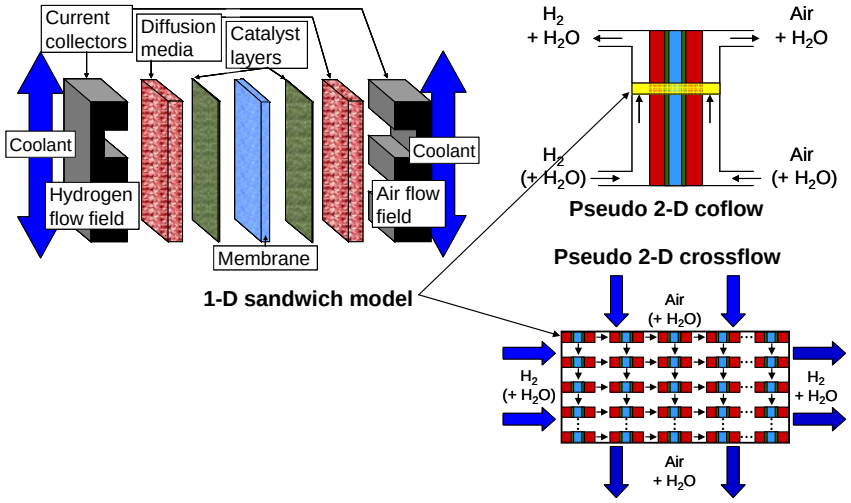

Figure 3. Schematic of the modeling domain where the 1-D (through-plane) sandwich model is run along the gas channel in coflow or in a 2-D matrix in crossflow. Each 1-D model segment contains a different membrane or cathode-catalyst-layer thickness as given by the distributions in 61HFigure 2.

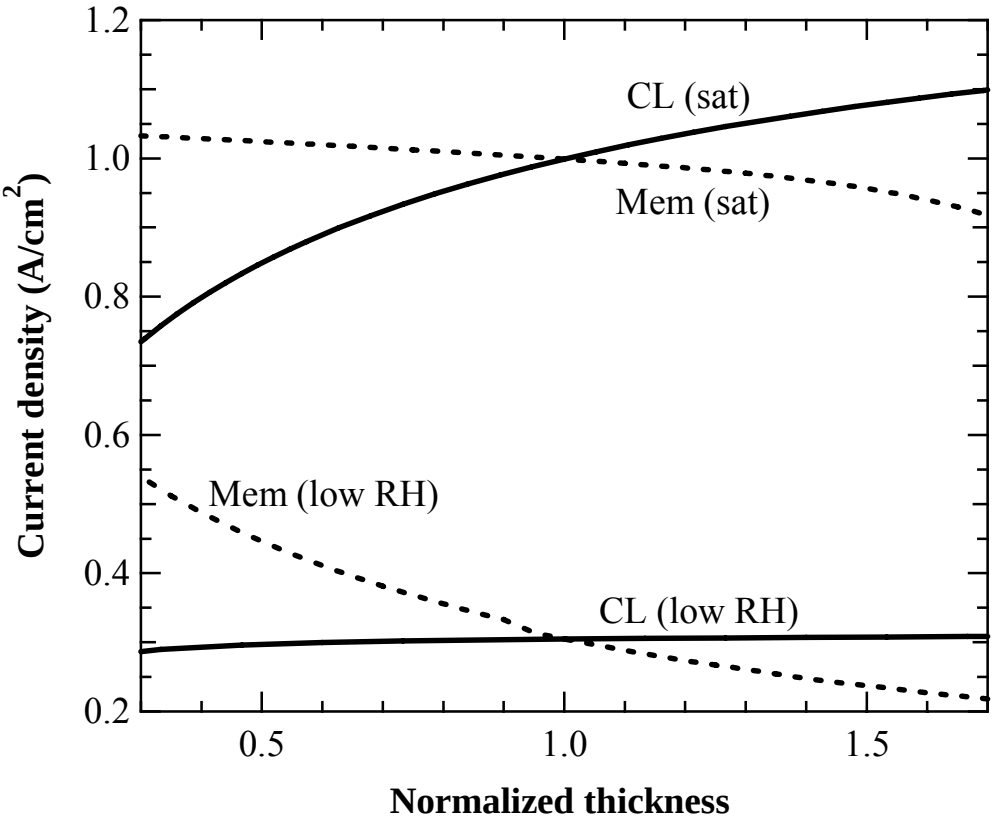

Figure 4. Impact of catalyst-layer (solid) and membrane (dashed) thickness on the cell current density at 0.6 V. Each thickness is uniform along the gas channel, and the normalization is with respect to the average thicknesses of 30 and 13.5 μm for the membrane and catalyst layer, respectively. The two sets of lines indicate saturated and 25 % relative-humidity feeds.

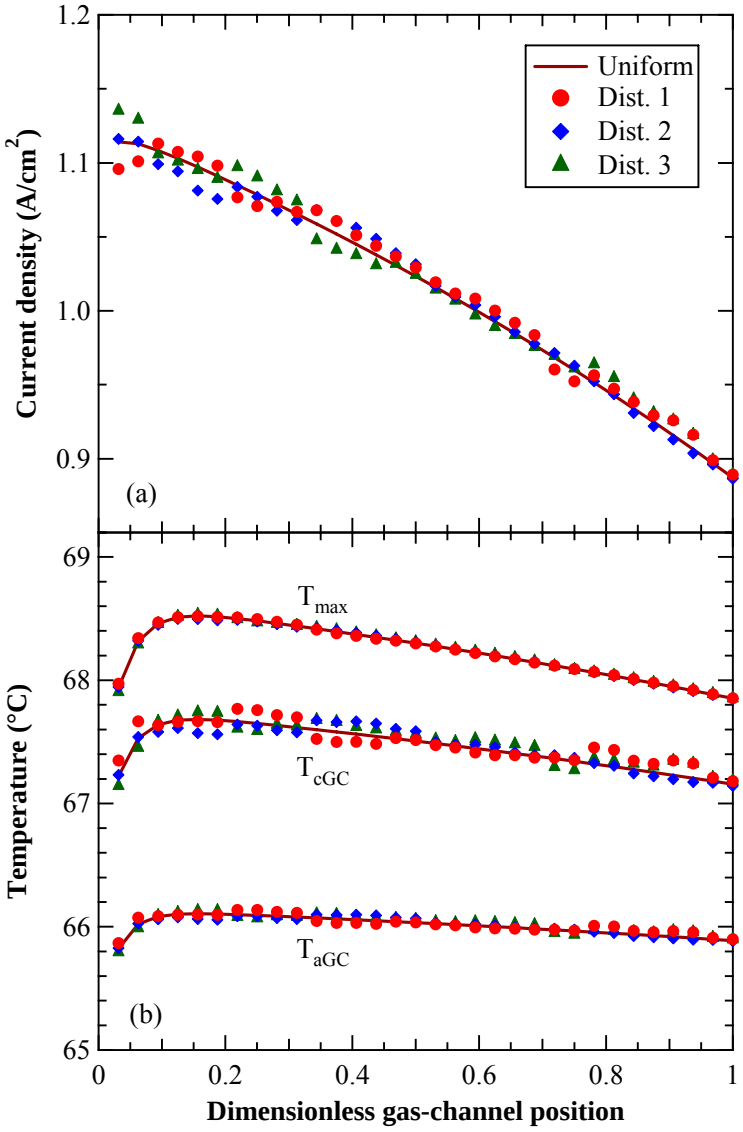

Figure 5. Along-the-channel values for the (a) current density and (b) maximum and anode- and cathode-gas-channel temperatures as a function of membrane-thickness distribution at 0.6 V with saturated feeds. The distributions correspond to those shown in Figure 2, the solid line indicates a uniform thickness at a value of 30 μm

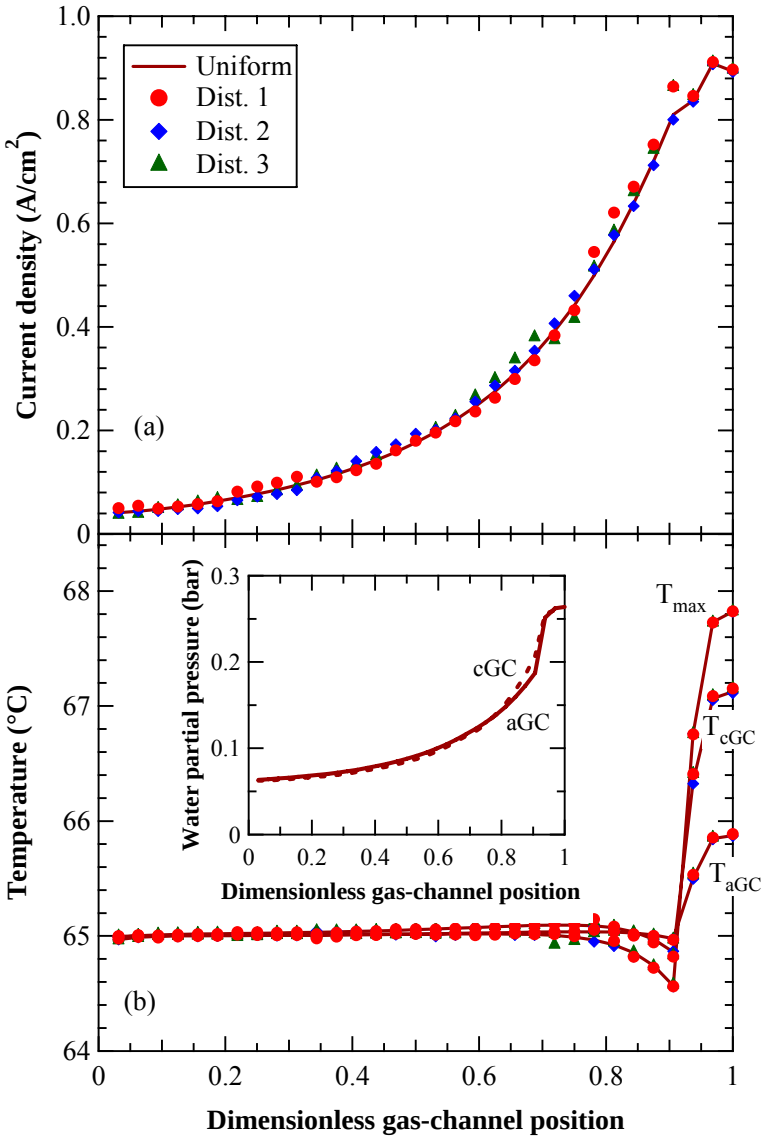

Figure 6. Along-the-channel values for the (a) current density and (b) maximum and anode- and cathode-gas-channel temperatures as a function of membrane thickness distribution at 0.6 V with 25 % relative-humidity feeds. The distributions correspond to those shown in Figure 2, the solid line indicates a uniform thickness at a value of 30 μm, and the coolant temperature is 65°C. The inset graph in (b) shows the along-the-channel water partial pressure in the anode and cathode gas channels.

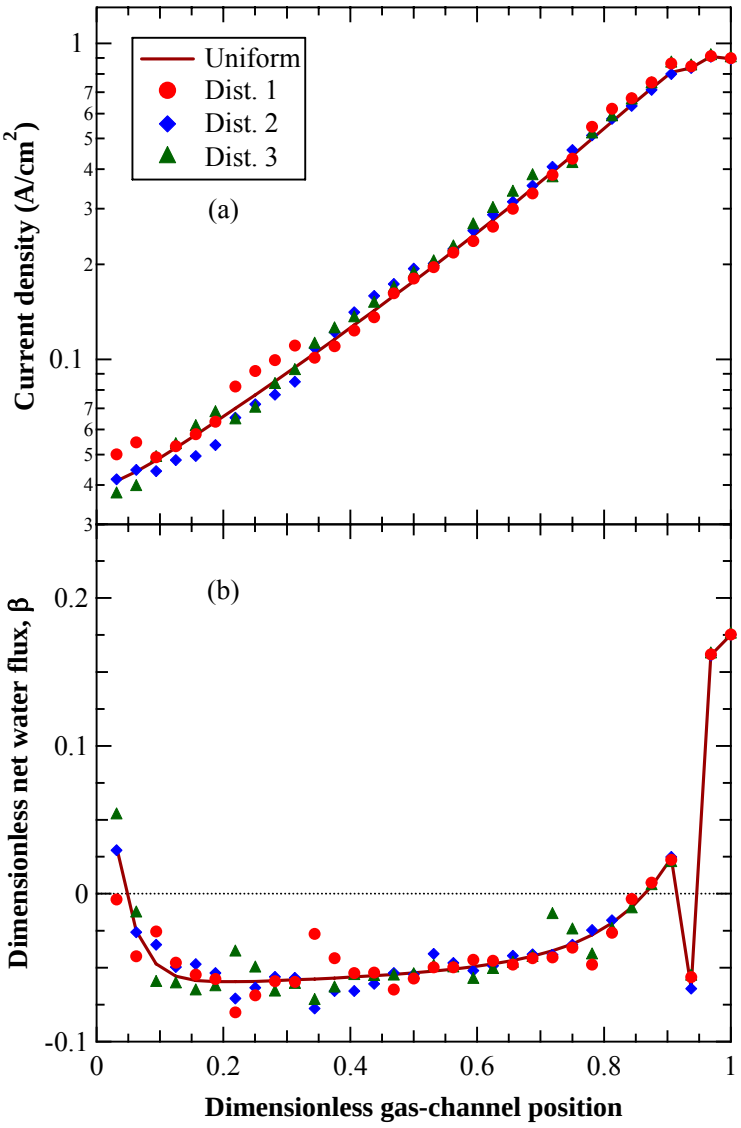

Figure 7. Along-the-channel values for the (a) current density and (b) dimensionless net water flux in the membrane, β, as a function of membrane thickness distribution at 0.6 V with 25 % relative-humidity feeds. (a) is the same as Figure 6(a) except on a logarithmic scale to emphasize the relative errors. The distributions correspond to those shown in Figure 2, and the solid line indicates a uniform thickness at a value of 30 μm.

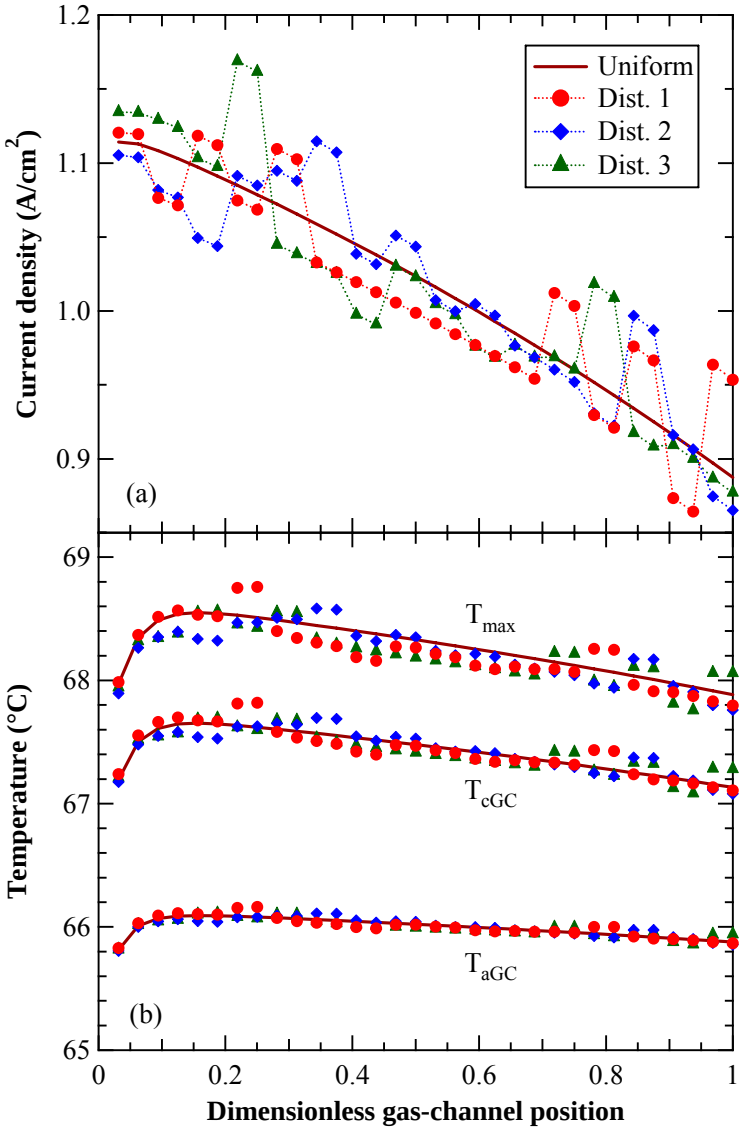

Figure 8. Along-the-channel values for the (a) current density and (b) maximum and anode- and cathode-gas-channel temperatures as a function of catalyst-layer thickness distribution at 0.6 V with saturated feeds. The distributions correspond to those shown in 66HFigure 2, *the* solid line indicates a uniform thickness at a value of 13.5 □m, and the coolant temperature is 65°C.

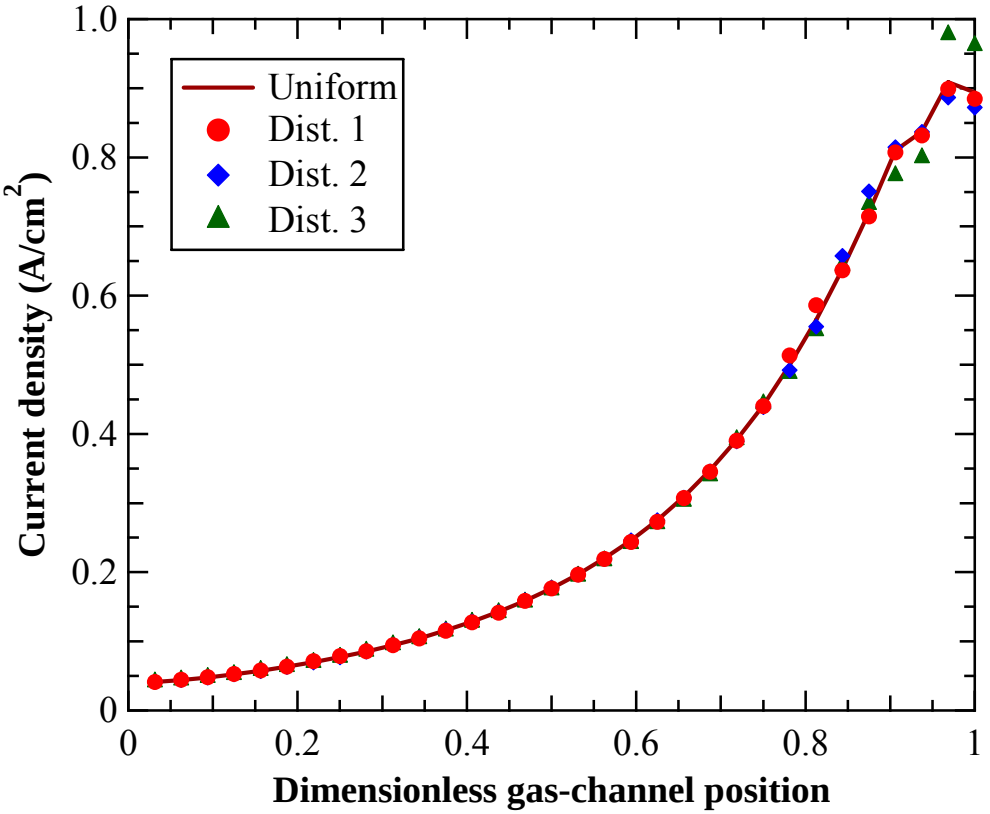

Figure 9. Along-the-channel values for the current density as a function of catalyst-layer thickness distribution at 0.6 V with 25 % relative-humidity feeds. The distributions correspond to those shown in Figure 2, and the solid line indicates a uniform thickness at a value of 13.5 μm.

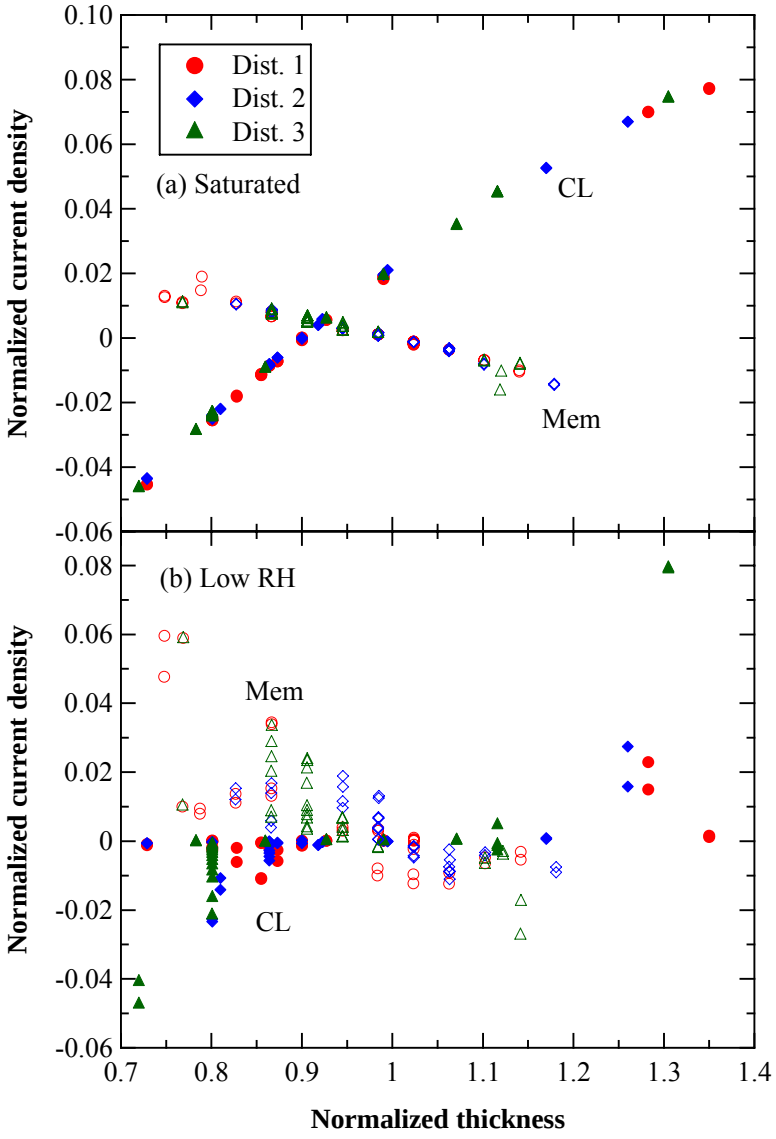

Figure 10. Normalized current density as a function of normalized layer thickness from simulation for both the membrane (hollow symbols) and catalyst-layer (filled symbols) thickness distributions at 0.6 V with *(a)* saturated and (b) 25 % relative-humidity feeds. The normalization is done with respect to the along-the-channel-value deviations from the uniform-thickness-distribution cases

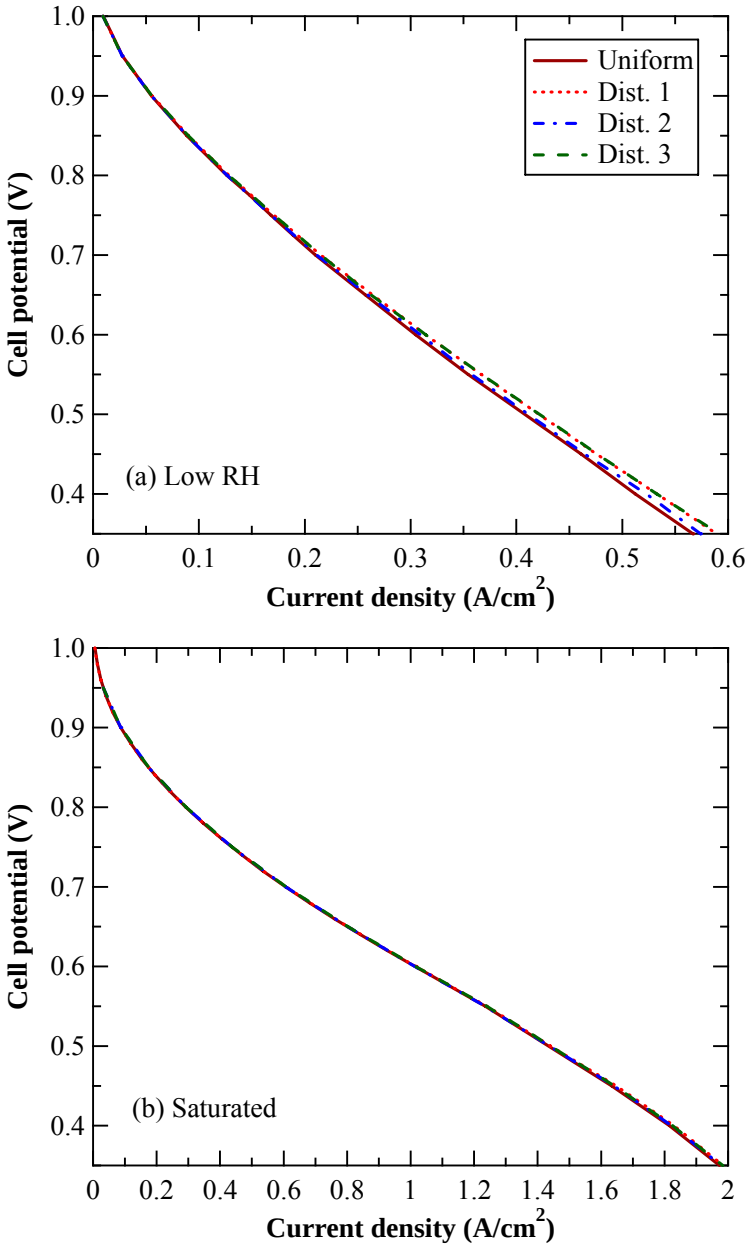

Figure 11. Polarization curves for the four membrane-thickness distributions for both the (a) 25 % relative-humidity and (b) saturated feed cases.